Molecular Therapy
Methods & Clinical Development
Original Article

Iron oxide-coupled CRISPR-nCas9-based genome editing assessment in mucopolysaccharidosis IVA mice

Andrés Felipe Leal,[1,2] Betul Celik,[2,3] Nidhi Fnu,[2,3] Shaukat Khan,[2] Shunji Tomatsu,[2,3,4,5] and Carlos Javier Alméciga-Díaz[1]

[1]Institute for the Study of Inborn Errors of Metabolism, Faculty of Science, Pontificia Universidad Javeriana, Bogotá DC 110231, Colombia; [2]Nemours Children's Health, Wilmington, DE 19803, USA; [3]Faculty of Arts and Sciences, University of Delaware, Newark, DE 19716, USA; [4]Department of Pediatrics, Graduate School of Medicine, Gifu University, Gifu 501-1193, Japan; [5]Department of Pediatrics, Thomas Jefferson University, Philadelphia, PA 19144, USA

Mucopolysaccharidosis (MPS) IVA is a lysosomal storage disorder caused by mutations in the *GALNS* gene that leads to the lysosomal accumulation of keratan sulfate (KS) and chondroitin 6-sulfate, causing skeletal dysplasia and cardiopulmonary complications. Current enzyme replacement therapy does not impact the bone manifestation of the disease, supporting that new therapeutic alternatives are required. We previously demonstrated the suitability of the CRISPR-nCas9 system to rescue the phenotype of human MPS IVA fibroblasts using iron oxide nanoparticles (IONPs) as non-viral vectors. Here, we have extended this strategy to an MPS IVA mouse model by inserting the human GALNS cDNA into the ROSA26 *locus*. The results showed increased GALNS activity, mono-KS reduction, partial recovery of the bone pathology, and non-IONPs-related toxicity or antibody-mediated immune response activation. This study provides, for the first time, *in vivo* evidence of the potential of a CRISPR-nCas9-based gene therapy strategy for treating MPS IVA using non-viral vectors as carriers.

INTRODUCTION

Mucopolysaccharidosis (MPS) IVA is a lysosomal storage disorder (LSD) caused by mutations in the *GALNS* gene.[1] Impaired GALNS activity leads to lysosomal accumulation of glycosaminoglycans (GAGs), chondroitin 6-sulfate, and keratan sulfate (KS).[2] Consequently, patients suffering from MPS IVA present progressive skeletal dysplasia and cardiovascular and respiratory complications.[2] Enzyme replacement therapy (ERT) is the only approved drug for treating MPS IVA.[3,4] Although ERT for MPS IVA has shown positive outcomes in the 6-min walk test and endurance, suggesting a positive cardiopulmonary impact,[5] ERT has a short life,[6] low effect in oxidative stress phenotype recovery,[7] poor bone improvement,[8] and high cost.[9]

Hematopoietic stem cell transplantation has been proposed as a therapeutic alternative; however, its use in clinical practice is not extended to all MPS IVA patients.[10] In contrast, substrate degradation therapy[11] and pharmacological chaperones[12,13] have been evaluated as potential treatment alternatives. Since MPS IVA is a monogenic disease, gene therapy (GT)-based strategies are among the most promising alternatives since they can provide a long-term expression of the *GALNS* transgene.[14–16] Previous reports have shown the suitability of GT in MPS IVA mice models using viral vectors.[17–20] Nevertheless, it is well known that the use of viral vectors remains challenging due to the development of immune response, oncogenesis activation, low package capacity, and vector dilution, among others.[21] Thus, the search for new GT approaches remains a priority.

The use of the CRISPR and CRISPR-Cas9 system as a biotechnological tool for genome editing has opened a new horizon for genetic diseases in the last decade.[22] The CRISPR-Cas9 system leads to inserting DNA sequences at virtually any genomic region with surgical precision,[23,24] overcoming the random insertion observed with some viruses.[21,25] Although the CRISPR-Cas9 system has been successfully tested in some LSDs, such as Gaucher disease,[26] GM2 gangliosidoses,[27,28] metachromatic leukodystrophy,[29] and MPS I,[30] it has not been evaluated *in vivo* for MPS IVA.

We recently reported the suitability of a CRISPR-Cas9 strategy by using a Cas9 nickase (nCas9) to insert an expression cassette containing GALNS cDNA into the AAVS1 *locus* in human MPS IVA fibroblasts using iron oxide nanoparticles (IONPs) as non-viral vectors.[31] The results showed a long-term GALNS expression, lysosomal mass recovery, and mitochondrial-derived reactive oxygen species amelioration in the human MPS IVA fibroblasts, supporting the use of CRISPR-nCas9 as a promising alternative for treating MPS IVA.

Received 24 August 2023; accepted 3 November 2023;
https://doi.org/10.1016/j.omtm.2023.101153.

Correspondence: Shunji Tomatsu, Nemours Children's Health, Wilmington, DE 19803, USA.
E-mail: shunji.tomatsu@nemours.org
Correspondence: Carlos Javier, Institute for the Study of Inborn Errors of Metabolism, Faculty of Science, Pontificia Universidad Javeriana, Bogotá DC 110231, Colombia.
E-mail: cjalmeciga@javeriana.edu.co

Similar results were obtained for GM2 gangliosidoses, confirming that this strategy is a potential alternative for treating LSDs.[27]

To extend our previous *in vitro* results, in this study, we evaluated an IONPs-coupled CRISPR-nCas9 system in a human GALNS-tolerant MPS IVA mouse (MTOL) model.[32] The CRISPR-nCas9 was designed to target the ROSA26 *locus* to mediate the wild-type (WT) human GALNS cDNA insertion into the mouse genome. After the *in vitro* validation, the IONPs-coupled CRISPR-nCas9 system was intravenously administered to newborn MTOL mice to determine the efficacy of this system in correcting the biochemical and pathology alterations of MPS IVA.

RESULTS

CRISPR-Cas9 design and *in vitro* validation

Double nCas9-dependent nicking leads to the knock-in of an expression cassette-carrying GALNS cDNA into the ROSA26 locus

Two single guide RNAs (sgRNAs) targeting the ROSA26 *locus* were designed and cloned into the CRISPR-nCas9 plasmid. Plasmids were transfected into NIH/3T3 mouse fibroblasts using lipofectamine LTX (LP-LTX) (Figures 1A and 1B). After transfection, genomic DNA was used for PCR amplification using primers flanking the expected ROSA26 on-target region, and a ∼0.9-kb PCR product was obtained (Figure 1C). The PCR products were then treated with T7 enzyme to detect mismatch alignments. As observed in Figure 1D, by transfecting the CRISPR-nCas9 plasmid containing either AS- or S-sgRNA, no Cas9 cut was observed. However, when both sgRNAs were cloned into the CRISPR-nCas9 plasmid, 56% on-target cut was obtained on fluorescence-sorted NIH/3T3 cells (Figure 1D). These results were further confirmed by Sanger sequencing (Figure 1E). Insertions and deletions (Indels) were mainly represented by deletions (Figure S1).

Off-target evaluation of the top ten predicted sequences by Sanger sequencing showed no significant changes between untreated and treated NIH/3T3 fibroblasts (Figure S2). In contrast, homologous recombination assays showed an expected band of about 1.5 kb in NIH/3T3 cells transfected with both CRISPR-nCas9 and donor ROSA26:GALNS plasmids, suggesting the insertion of Donor ROSA26:GALNS into ROSA26 *locus* (Figure S3). Sanger sequencing confirmed the knock-in of the donor template (Figure S3). Overall, these results suggest a highly efficient Cas9-dependent on-target cutting that leads to knock-in of donor ROSA26:GALNS with undetectable off-target effects.

The IONPs-coupled CRISPR-nCas9 system leads to phenotype recovery in long-term-treated MTOL fibroblasts

Before conducting the *in vitro* evaluation of the CRISPR-nCas9 system, a characterization of the physical properties of the IONPs was carried out. Empty IONPs and the IONPs-coupled CRISPR-Cas9 system (CRISPR-nCas9 and donor ROSA26:GALNS plasmids) showed a mean size of 174.4 nm and 191 nm, respectively, as well as a Z-potential of +44.9 and +39.5 mV, respectively (Figure 2A). Moreover, IONPs prevented the enzymatic degradation of CRISPR-nCas9-associated plasmids in the *Dpn*I assays (Figure 2B), suggesting that electrostatic interactions between positively charged IONPs and negative pDNA may lead to efficient transport and delivery of the CRISPR-nCas9 system in both *in vivo* and *in vitro* assays.

MTOL fibroblasts were transfected with IONPs or LP-LTX, followed up to 1 month after treatment, and analyzed for GALNS activity and lysosomal mass. Untreated MTOL fibroblasts showed undetectable intra- and extracellular GALNS activity. After treatment with the CRISPR-nCas9 system using LP-LTX (Figure 2C), the extracellular GALNS activity increased up to WT levels (∼0.0009 U/mL) compared with untreated fibroblast ($p \leq 0.0001$). Transfection of the CRISPR-nCas9 system using IONPs led to a GALNS activity increase of 77% of WT levels (Figure 2C). Consistently, intracellular GALNS activity increased up to 63.4% and 61.8% of WT levels after transfection of the CRISPR-nCas9 system by using LP-LTX and IONPs, respectively (Figure 2D). Although an increase in GALNS activity was observed in MTOL fibroblasts transfected only with donor ROSA26:GALNS plasmid, those levels remained as low as 5% WT levels, suggesting that donor plasmid was lost as a consequence of the cell proliferation.

Regarding lysosomal mass, untreated MTOL fibroblasts showed a 2.5-fold increase in the Lysotracker signal compared with WT fibroblasts (Figure 3A). The lysosomal mass was significantly reduced after long-term CRISPR-nCas9 genome editing, with no significant differences compared to WT levels, suggesting normalization of this parameter (Figure 3A). Similar findings were observed in fluorescence microscopy (Figure 3B). Overall, these results indicate that inserting a human GALNS cDNA expression cassette into the ROSA26 *locus* may result in long-term GALNS expression and lysosomal mass normalization.

In vivo assessment of the IONPs-coupled CRISPR-nCas9 system

IONPs-coupled CRISPR-nCas9 failed to induce chronic toxicity in MTOL mice

Before long-term CRISPR-nCas9-based genome editing *in vivo* experiments, a biodistribution assessment was performed in 8-week-old animals using DiIC-labeled IONPs due to their convenience for autopsies compared with newborn mice. As observed in Figure 4A, *ex vivo* imagining analysis revealed that IONPs were distributed mainly to the liver, followed by the lung, muscles, spleen, and kidney. No radiance fluorescence was observed in the brain and heart.

To evaluate the potential chronic toxic effects of IONPs, alone or carrying the CRISPR-nCas9 and donor plasmids, blood samples collected at autopsy were assessed for hepatic and renal biomarkers, as well as iron homeostasis (Figures 4B–4E). After 12 weeks of treatment, no significant changes were observed in the hepatic (Figure 4B) or renal (Figure 4C) biomarkers tested. Consistently, hematoxylin and eosin staining revealed no noticeable histopathological changes (Figure 4D). Iron homeostasis was also unaffected (Figure 4E). Collectively, these results suggest that 2.5 μg IONPs carrying 3.8 μg pDNA are non-toxic in newborn MTOL mice.

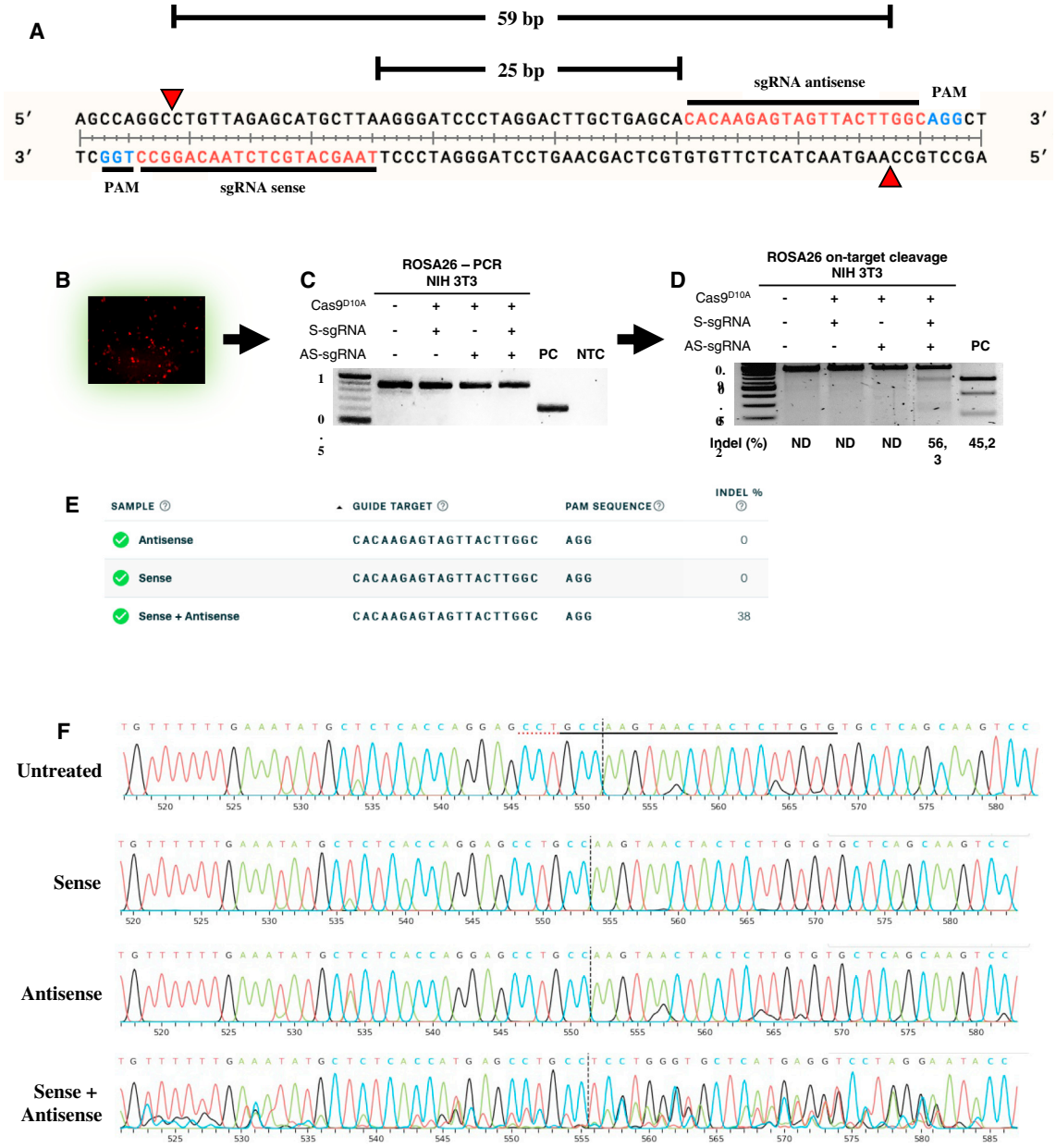

Figure 1. CRISPR-nCas9-based gene strategy for targeting the ROSA26 *locus*

The figure shows in (A), the schematic representation for two sgRNAs (red sequences) targeting the ROSA26 *locus*. The PAM sequences are in blue, while the red arrows indicate the predicted nCas9 nicking sites. An off-set 25 nucleotides were considered to avoid any steric hindrance. Notice that a PAM-out configuration was included for each RNP complex (Off-set: 59). In (B), epifluorescence microscopy pictures from NIH/3T3 cells (40×) transfected with AIO-mCherry plasmid containing both sense and antisense sgRNA sequences are shown. In (C), a PCR amplification of the ROSA26 *locus* shows an expected PCR product of ~0.9 kb. In (D), the indel frequency is detected by T7-dependent cleavage. In (E) and (F) is the trace decomposition from sorted NIH/3T3 cells transfected with either sense, antisense, or sense-antisense sgRNAs. Double picks are clearly observed when the cells are transfected with AIO-mCherry carrying both AS- and S-sgRNA sequences. PC, positive control; NTC, no template control.

IONPS-coupled CRISPR-nCas9 system led to long-term GALNS expression in MTOL mice

Although body weight changes in MTOL mice had not been reported as a significant feature in this MPS IVA model,[32] we observed a significant difference in body weight between WT (32.7 ± 0.77 g) and MTOL (28.8 ± 0.83 g) untreated mice after 12 weeks of follow up ($p = 0.0006$) (Figure 5A). These differences were not evident before 3 weeks after birth, although they increased after weaning.

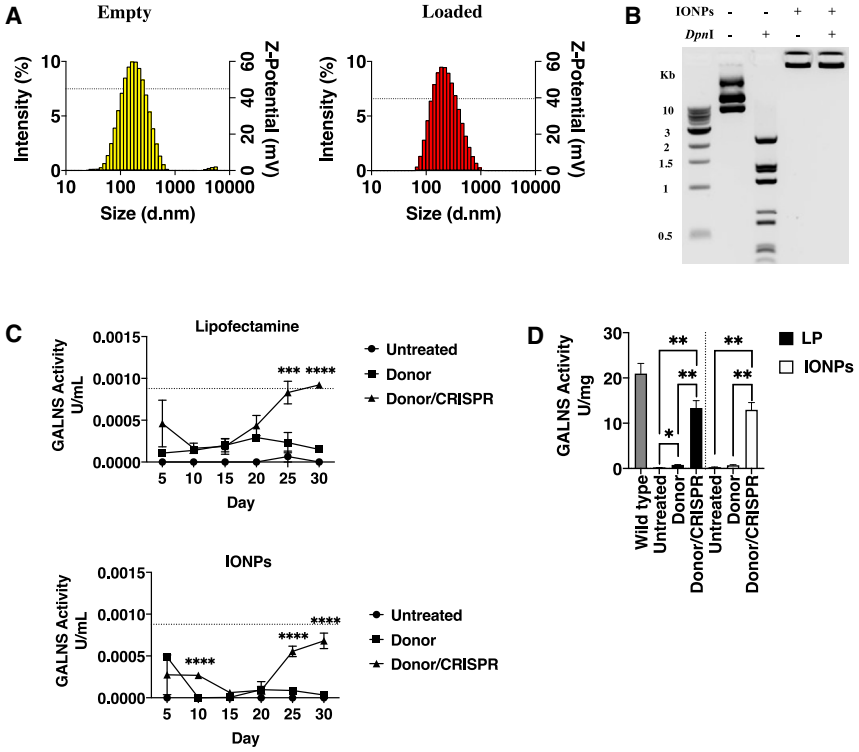

Figure 2. Physicochemical IONPs characterization and long-term GALNS expression in MTOL fibroblasts

(A) Dynamic light scattering (DLS) from IONPs for empty or loaded IONPs. The coupling of the CRISPR-nCas9-associated plasmids decreased the Z-potential (dotted line). (B) *Dnp*I digestion assay. Notice that pDNA is digested only when not complexed with IONPs (naked). (C) Extracellular GALNS activity (n = 5) was determined from culture media from MTOL fibroblasts transfected with lipofectamine (LP) or IONPs. The dotted line represents extracellular GALNS activity detected in WT fibroblasts. Notice that, by using lipofectamine as the carrier of the CRISPR-Cas9 system, GALNS activity increased over time, while by using IONPs, GALNS activity showed a decrease at 15 days post-transfection that was recovered after 25 days post-treatment. (D) Intracellular GALNS activity (n = 5). *p ≤ 0.05, **p ≤ 0.01, ***p ≤ 0.001, ****p ≤ 0.0001. Two-way ANOVA.

Even though the body weight was not affected upon administration of IONPs carrying Donor ROSA26:GALNS plasmid, at 12 weeks post-treatment, the body weight from MTOL mice increased up to 31.9 ± 1.4 g (p = 0.0197) and 30 ± 0.5 g (p = 0.049) when treated with the naked plasmids and the IONPs-coupled CRISPR-nCas9 system, respectively, compared with untreated MTOL mice (Figure 5A).

As previously reported,[17,32] untreated MTOL mice showed no GALNS activity on plasma or tissues (Figures 5B–5D). After treatment with the IONPs-coupled CRISPR-nCas9 system, the plasma GALNS activity initially increased from 0.5 ± 0.046 U/mL 5 weeks post-treatment up to 1.36 ± 0.206 U/mL at 12 weeks post-treatment, which correspond with 10.2% and 27.7% of WT levels (4.9 ± 0.253 U/mL), respectively (Figure 5B). Although IONPs-coupled donor ROSA26:GALNS did not arise on any detectable GALNS activity in plasma, the administration of the naked CRISPR-nCas9 system resulted in a significant GALNS activity increase (0.2 ± 0.088 U/mL, 4.1% WT levels), compared with untreated animals (Figure 5B), suggesting that plasmids could be taken up by cells in the absence of the IONPs. No changes in plasma GALNS activity were observed in MTOL treated with empty IONPs.

In contrast, the liver (75.4% WT levels), muscle (67.4% WT levels), spleen (34.8% WT levels), heart (57.2% WT levels), kidney (55.4% WT levels), and lung (47.8% WT levels) from MTOL mice treated with IONPs-coupled CRISPR-nCas9 system showed a significant increase in the GALNS activity at 12 weeks post-treatment compared with untreated MTOL mice (Figure 5C). A significant GALNS activity increase was also noticed in the liver (13.3% WT levels) and kidney (9.7% WT levels) of MTOL mice injected with the naked CRISPR-nCas9 system, compared with untreated ones.

For the tibia and trachea, GALNS enzyme activity from the IONPS-coupled CRISPR-nCas9 system MTOL-treated mice increased to 6.8% and 12.6% of WT levels, respectively. In contrast, no activity increase was observed in untreated MTOL mice or treated with the naked plasmids or the IONPs-coupled donor ROSA26:GALNS plasmid (Figure 5D). Finally, no detectable GALNS activity was observed in the brain of any treated mouse (data not shown).

CRISPR-nCas9-dependent long-term GALNS expression led to a significant decrease in the mono-sulfated KS accumulation

A significant mono-sulfated KS increase was observed in plasma, liver, and bone from untreated MTOL animals compared with WT mice (Figure 6), suggesting substrate accumulation due to the absence of GALNS activity.[17,32] Consistent with GALNS activity levels, a significant mono-sulfated KS reduction was also observed in plasma (Figure 6A), liver (Figure 6B), and humerus (Figure 6C) of MTOL mice treated with the IONPs-coupled CRISPR-nCas9 system (Figure 6) compared with untreated MTOL mice, suggesting a positive impact of the CRISPR-nCas9-based GT. Even though mono-sulfated KS levels were not reduced significantly in plasma samples from naked CRISPR-nCas9-treated mice, a significant reduction of mono-sulfated KS levels was detected in the liver of naked CRISPR-nCas9-treated mice, consistent with the GALNS levels observed in the liver of those animals. This behavior was not observed for the humerus of naked CRISPR-nCas9-treated mice.

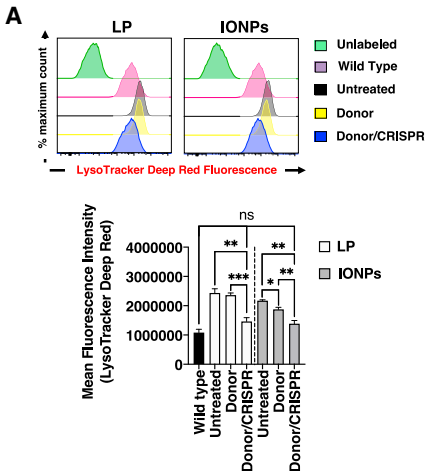

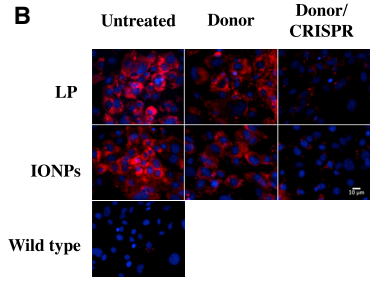

Figure 3. Lysosomal mass evaluation in long-term MTOL-treated fibroblasts

(A) (Left) Representative histograms from MTOL fibroblasts edited with CRISPR-nCas9 using LP-LTX or IONPs as carriers. The MFI from the left is shown at the bottom (n = 6). Note that, upon long-term edition, using either LP or IONPs, no significant difference with WT levels was obtained, suggesting a normalization of the lysosomal mass in MTOL fibroblasts. (B) Epifluorescence microscopy for lysosomal mass (red staining) and nucleus (blue staining). Scale bar, 10 μm. *p ≤ 0.05, **p ≤ 0.01, ***p ≤ 0.001. Two-way ANOVA.

IONPs-coupled CRISPR-nCas9 system positively impacted pathological findings in the tibia

As previously reported,[17] pathology analysis of the tibia from untreated MTOL mice showed a 1.7-, 1.5-, and 2.0-fold increase in chondrocyte size placed on the growth plate, articular cartilage, and meniscus, compared with WT mice, respectively (Figure 7). Bone regions were positively impacted in MTOL mice treated with the IONPs-coupled CRISPR-nCas9 system. Chondrocyte size improvement in the growth plate and meniscus did not reach WT levels. In contrast, chondrocyte size in the articular cartilage was not different from that observed in WT mice (Figure 7B). Likewise, a vacuolization decrease was also observed in chondrocytes in the growth plate, articular cartilage, and meniscus (Figure 7). Furthermore, vacuolization and columnar structure in pathological findings were scored in the knee joint as previously described.[33] In the tibia, chondrocyte vacuolization was significantly improved in IONPs-coupled CRISPR-nCas9 system-treated MTOL mice compared with untreated ones in the growth plate and articular cartilage. At the same time, a slight non-significant recovery of the column structure was observed in these regions (Table S4). No significant improvement was detected in the femur, ligament, or meniscus (Table S4). Overall, these results suggested that the IONPs-coupled CRISPR-nCas9 system positively impacts key pathological findings in the MPS IVA mouse model.

No anti-GALNS nor anti-nCas9 antibodies response was achieved upon nCas9 treatment

To determine the potential impact of the immune response on the outcome of the CRISPR-nCas9 system, anti-GALNS and anti-nCas9 antibodies were evaluated. As expected, no significant increase in anti-GALNS IgG was observed after 12 weeks of treatment in MTOL mice (Figure 8A), supporting the immunotolerance to human GALNS of this MPS IVA model.[32] Under the experimental conditions tested in this study, no increase in anti-nCas9 antibodies was observed in MTOL mice treated with naked plasmids or the IONPS-coupled CRISPR-nCas9 (Figure 8B) regardless of the persistence of nCas9 plasmid (0.003 ± 0.0009 copies per diploid cell) in the liver of MTOL animals after 12 weeks of treatment (Figure S4). We did not observe copies of the donor template or nCas9 plasmid in the testes of the MTOL mice treated after 12 weeks post-treatment (data not shown).

DISCUSSION

Despite the promising achievements reported for the CRISPR-Cas9 system as a potential strategy for treating LSDs, such as MPS I, GM2 gangliosidoses, Gaucher disease, and metachromatic leukodystrophy,[26–30] it has not been tested in animal models of MPS IVA. In this study, a novel IONPs-coupled CRISPR-nCas9 system targeting the ROSA26 *locus* was developed and evaluated *in vivo* using human GALNS-tolerant MPS IVA mice.

The *in vitro* validation demonstrated a significant increase in GALNS enzyme after one-month post-treatment (Figure 3), which recovered the lysosomal mass in MPS IVA fibroblasts to those observed in WT fibroblasts. These findings were similar to those achieved previously in human MPS IVA fibroblasts with a similar approach but targeting the AAVS1 *locus*.[31] Compared with GALNS activity observed in human MPS IVA fibroblasts after one-month post-treatment, MTOL fibroblasts resulted in higher GALNS activity, both intracellularly (∼40% ∼63% WT levels, respectively) and extracellularly (∼6% vs ∼70% WT levels, respectively).[31] Since the expression cassette was the same in both human and mouse fibroblasts, the differences observed could be attributed to the on-target Cas9 efficiency. For instance, a 56% on-target efficacy was observed for the ROSA26 *locus* (Figure 1D), while 37% on-target efficacy was observed for the AAVS1 *locus*,[31] supporting that either sgRNA design or intrinsic *locus* organization can influence the efficiency of the CRISPR-nCas9-based gene editing.[34–36]

Although IONPs have been previously evaluated for several diseases and magnetic resonance imagining aspects,[37,38] they have not been tested as a gene-delivering strategy in any LSD. IONPs-based drugs, such as Fereheme for treating iron deficiency anemia,[39] are currently approved for use in humans, given that they cause only minor adverse effects in humans due to their high biocompatibility.[37,40,41] IONPs are cleared naturally through the iron

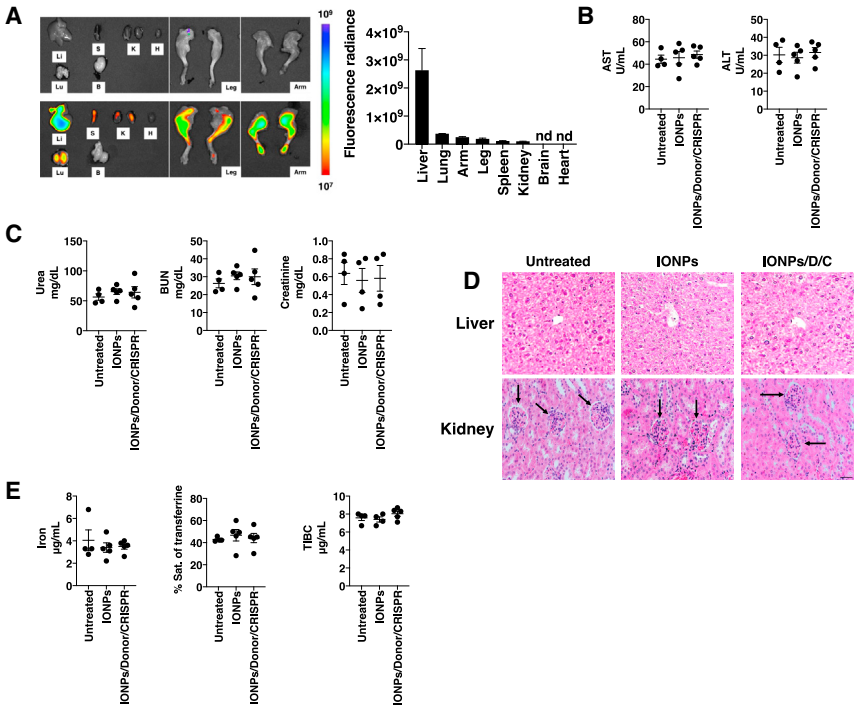

Figure 4. IONPs biodistribution and chronic toxicity evaluation in MTOL mice

(A) The upper panel represents tissues from untreated and treated animals. The bottom panel shows the mean (n = 4) of fluorescence radiance for each tissue evaluated. Note that IONPs are primarily accumulated in the liver (Li). H, heart; K, kidney; Lu, lung; S, spleen. (B) Brain. nd, not detectable. The liver- and kidney-related toxicity biomarkers are shown in (B) and (C). (D) shows hematoxylin and eosin staining for liver and kidney samples from untreated (n = 4), empty IONPs (n = 5), and IONPs/donor/CRISPR (IONPs/D/C, n = 5) treated MTOL mice. In the kidney, black rows show glomeruli. Scale bar, 100 µm. In (E), the evaluation of iron homeostasis is presented.

metabolism pathway.[40,42] IONPs used in this study were characterized for basic parameters of hydrodynamic size and charge, showing that after loading, they resulted in 191 nm and +39.5 mV, respectively (Figure 2A), and mainly accumulated into the liver (Figure 4A), which agreed with previous reports using the same IONPs,[43] and similar ones.[42,44] Kupffer cell-mediated phagocytosis seems to be responsible for the uptake of IONPs larger than 100 nm.[45] Additionally, IONPs were observed in the lungs, muscles, spleen, and kidneys. Consequently, the *in vivo* experiments were conducted without an external magnetic field to allow an IONPs distribution of the CRISPR-nCas9 system throughout the body. This strategy led to the overexpression of GALNS in different tissues, not only the liver. After 12 weeks post-treatment, MTOL mice showed no significant change in liver and renal biomarkers or serum iron levels compared with untreated ones (Figure 4), indicating that a dose of 2.5 µg IONPs-coupled CRISPR-nCas9 system did not induce any chronic toxicity. These results agree with previous reports using IONPs,[46,47] supporting the suitability of these nanoparticles as potential non-viral vectors for gene editing.

Under the experimental conditions tested in this study, a significant increase in GALNS activity was achieved in plasma (~28% WT levels) and all the evaluated tissues (between ~7% and ~75% WT levels) (Figure 5). Even though IONPs were not accumulated in the heart, we observed a significant GALNS increase in the heart suggesting that cross-correction occurred.[48,49] Recently, Sawamoto et al.,[17] using an AAV8 vector for the transduction of the GALNS cDNA in MTOL mice, showed supraphysiological GALNS levels in plasma (4- to 19-fold), liver (~6,250% WT levels) and spleen (~316% WT levels); physiological levels in the heart; and levels lower than 20% of WT levels in the lung, kidney, and bone. Similar approaches were reported by Bertolini et al., 2021 on a novel MPS IVA rat model treated with AAV9 for delivering a rat WT GALNS cDNA.[20] In this study, authors found complete normalization of the GALNS activity (i.e., WT levels) in the serum of MPS IVA rats after four months post-treatment. Also, AAV9-GALNS resulted in the prevention of bone and cartilage alterations and the correction of the tracheal and cardiac pathological findings. Although GALNS activity from both AAV-based studies is significantly higher than that observed in the present study, a comparable mono-sulfated KS reduction in the liver was achieved (Figure 6), suggesting that even non-supraphysiological GALNS levels can also positively impact the natural history of MPS IVA when early treatment is established.[50] In fact, mild phenotypes have been reported in patients with a slight residual plasma GALNS activity (1.3%–13.3%) compared with healthy control levels.[51–54] Consequently, we hypothesize that the enzyme activity achieved in this study could also positively impact some features of the MPS IVA. In addition, a slight improvement in pathology was also observed in the tibia growth plate, meniscus, and articular cartilage from MTOL mice treated with the IONPs-coupled CRISPR-nCas9 system (Figure 7).

Although AAV-based GT led to higher enzyme activities than observed with IONPs in rodents, essential safety concerns such as the pre-existing anti-AAV antibodies are still to be overcome in humans.[55,56] Even though some immunosuppression regiments can be implemented in patients during AAV GT to blunt T cell responses,[56,57] evidence suggests that some patients can reject the therapy and develop hepatotoxicity.[58,59] A clinical trial (NCT03199469) aimed to treat X-linked myotubular myopathy (XLMTM) through the administration of an AAV8 for expressing MTM1 (deficient protein in XLMTM), resulted in the tragic death of three children, suggesting that viral vectors safety profile still to be covered more. Likewise, a recent report also showed the death of a patient with

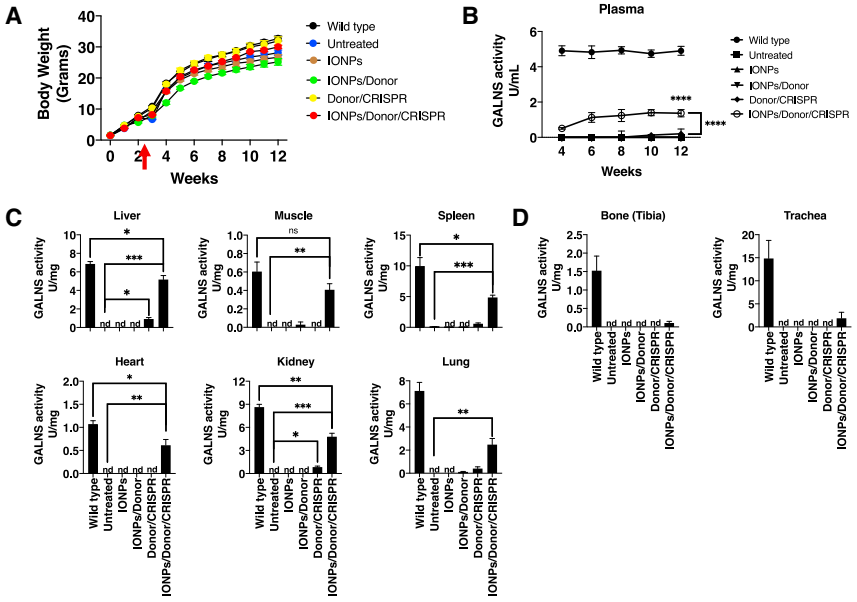

Figure 5. Impact of the CRISPR-nCas9 system in the body weight and long-term GALNS expression in MTOL mice

(A) Body weight from MTOL mice under different experimental conditions. Note that differences between experimental groups are most evident after weaning (red row). In (B), GALNS activity in plasma is shown, while (C) and (D) show tissues with significant and non-significant GALNS activity increase, respectively, from WT (n = 5), untreated (n = 5), empty IONPs (n = 5), IONPs/donor (n = 4), donor/CRISPR-nCa9 (n = 3), IONPs/donor/CRISPR (n = 5) treated MTOL mice. *p ≤ 0.05, **p ≤ 0.01, ***p ≤ 0.001. Two-way ANOVA.

Duchenne's muscular dystrophy after high-dose rAAV9 GT.[60] Instead, as previously discussed, IONPs safety profiles offer higher biocompatibility since they can be metabolized via the iron metabolism pathway.[40,42]

The results from this study revealed that the IONPs-coupled CRISPR-nCas9 system led to a higher enzyme activity recovery compared with previous findings with liposomes for delivering the CRISPR-Cas9 system to MPS I, where about 6% of WT IDUA activity was observed in plasma.[30] Moreover, GALNS activity levels were higher than those obtained during *ex vivo* CRISPR-Cas9 GT in MPS I mice, in which serum activity levels of ∼11.3% of WT levels were obtained.[61] Nevertheless, *ex vivo* CRISPR-Cas9 GT displays a better outcome in some peripheral tissues, such as the spleen (∼167.5% vs ∼34.8% WT levels, respectively) and brain (6.8% vs undetectable, respectively) compared with the approach evaluated in this study. *Ex vivo* findings can be rationally explained since HSC-derived macrophages and microglia can reach organs such as the brain.[62,63]

The immune response continues to be a challenge for several strategies, including CRISPR-Cas9-based GTs, since the presence of neutralizing antibodies can decrease the effectiveness of such therapies.[64,65] Anti-Cas9 antibodies have been identified in healthy individuals exposed to *Streptococcus pyogenes* during childhood.[65,66] Anti-Cas9 immune response represents a major concern in GT focused on LSDs, as pro-inflammatory events are well described in this group of disorders.[67–69] By treating newborn mice with the IONPs-coupled CRISPR-nCas9 system, no significant increase in anti-nCas9 antibodies was observed compared with untreated MTOL mice (Figure 8B), despite the nCas9 persistence observed in vector copy number experiments (Figure S4B). These findings are consistent with CRISPR-Cas9-based GT reports for hemophilia B and Duchenne muscular dystrophy, where antibodies against Cas9 were negligible when newborn mice were treated.[70,71] Despite these promising results, anti-Cas9 $CD8^+$ cytotoxic T lymphocytes (CTLs) have also been identified in healthy individuals.[65] Further experiments should be performed to determine the presence of specific anti-Cas9 CTLs and the proinflammatory profile after CRISPR-nCas9 treatment.

Even though results from this study revealed for the first time the potential of the IONPs-coupled CRISPR-nCas9 for treating MPS IVA, further experiments including a higher number of animals as well as 4-week-old mice should be conducted to test the full effectiveness of this strategy. In this regard, MPS IVA diagnosis is often not made at birth as they seem unaffected, and some biomarkers, such as total urine GAGs, can even be normal.[72] Consequently, novel therapeutical alternatives, including GT, will be evaluated in clinical trials involving young or adult MPS IVA patients.

In conclusion, the CRISPR-nCas9 system targeting the ROSA26 *locus* developed in this study leads to the *knock-in* of an expression cassette containing the human GALNS cDNA, leading to phenotype correction in MTOL fibroblasts using IONPs as non-viral vectors. Likewise, the *in vivo* assessment positively impacts GAGs accumulation and pathological findings with a non-significant anti-nCas9 humoral immune response or IONPs-coupled CRISPR-nCas9-associated toxicity. Overall, these results strongly suggest that IONPs-coupled CRISPR-nCas9 can be a promising alternative for treating MPS IVA.

MATERIALS AND METHODS

Mammalian cell culture

Mouse NIH/3T3 cells were gently donated by Professor Juan Carlos Cruz from the Biomedicine Engineering Department, Universidad de Los Andes. Cells were maintained in DMEM (Gibco) supplemented with 10% fetal bovine serum (FBS) (Gibco). At birth, skin mouse MPS IVA fibroblasts were isolated from human GALNS-tolerant MPS IVA mice and cultured in DMEM, 15% non-inactivated FBS. Skin mouse fibroblasts isolated from WT C57BL/6 mice were included as normal controls. Cells were maintained with

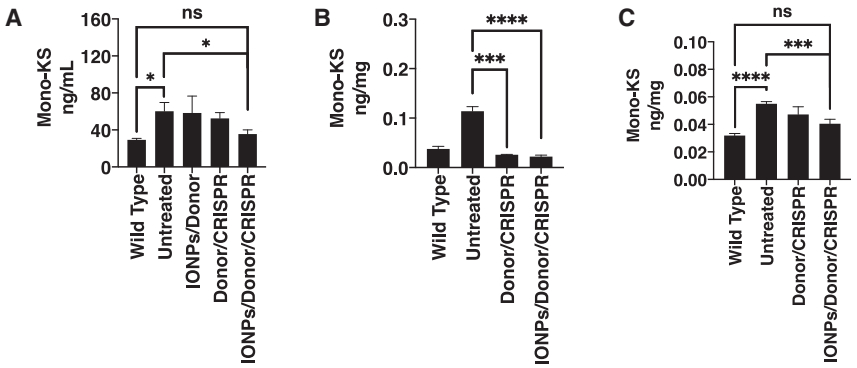

Figure 6. KS levels in MTOL mice

(A) KS levels detected in plasma samples. Note a non-significant difference in the KS levels from IONPs/Donor/CRISPR treated MTOL mice compared with WT mice. (B) KS levels in liver samples. Note that either naked or IONPs-coupled CRISPR-nCas9 resulted in a significant KS reduction compared with untreated MTOL mice. (C) KS levels in the humerus. WT (n = 5), untreated (n = 5), empty IONPs (n = 5), IONPs/donor (n = 3), donor/CRISPR (n = 3), BS IONPs/donor/CRISPR (n = 5). *p ≤ 0.05, ***p ≤ 0.001, ****p ≤ 0.0001. Two-way ANOVA.

supplemented DMEM plus 100 U/mL penicillin and 100 μg/mL streptomycin (Gibco) and incubated in a humidified atmosphere containing 5% CO_2. The assays were carried out using cells in passages between 1 and 3 after thawing.

Molecular strategy design and validation in NIH3T3cells

sgRNA design and cloning

Two sgRNA (Table S1) were designed to target the ROSA26 *locus* (NCBI: NC_000072.7). On- and off-target sequences were predicted using Benchling, Cas Off-finder, and Off-Spotter software (Table S2).[34] sgRNAs were obtained from Macrogen Inc. as single oligonucleotides and cloned into the AIO-mCherry plasmid (Addgene: #74120), which carries a mutant version of Cas9 at the RuvC domain (D10A), using the Golden Gate strategy as described previously.[31] The resulting vector (AIO-mCherry:sgRNA, hereafter CRISPR-nCas9 plasmid) was transformed into *Escherichia coli* DH5α, purified, sequenced through Sanger, and analyzed by Chromas Pro and MEGA X software. Plasmids used *in vitro* and *in vivo* were produced by VectorBuilder Inc.

Donor ROSA26 plasmid

Two homologous recombination arms were designed according to the sgRNA sequences. Left and right arms flanking cytomegalovirus immediate-early enhancer/promoter, Kozak sequence, P2A, enhanced green fluorescent protein (EGFP), and bGH poly(A) signal sequence were synthesized by Gene Art (Thermo Fisher Scientific) (Figure S3A). Two enzyme restriction sequences for *Mfe*I and *Mlu*I were included between Kozak and P2A sequences for cloning GALNS cDNA. GALNS cDNA was obtained from a previous donor vector tested for the AAVS1 *locus*.[31] The resulting donor was verified through Sanger sequencing. Plasmids used *in vitro* and *in vivo* were produced by VectorBuilder Inc.

On- and off-target evaluations

A mismatch-based screening was used to detect the double nicking by nCas9 on the ROSA26 *locus*. For this, confluent NIH/3T3 cells were transfected or not with CRISPR-nCas9, according to previous reports.[30,64] The cells were harvested 48 h post-transfection to isolate genomic DNA (gDNA) using the Monarch Genomic DNA Purification Kit (New England Biolabs). The resulting gDNA was used for high-fidelity PCR with primers flanking targeting the ROSA26 *locus* predicted site (Table S3). The mismatches were recognized by T7 endo-nuclease-mediated PCR product digestion (EnGen Mutation Detection Kit, New England Biolabs) following the manufacturer's instructions. The digested PCR products were electrophoresed on 2% w/v agarose gel (Lonza) and documented with a Geldoc XR + system (Biorad). Indel percentage was calculated using the GelAnalyzer 19.1 software.

A Sanger-based sequencing was performed to confirm the screening performed via T7 assay and the off-target effects of the sgRNAs designed. Briefly, NIH/3T3 cells were sorted by fluorescence-activated cell sorting (FACS) after transfection with the CRISPR-nCas9 plasmids using the mCherry fluorescence (*Exc/Emi*: 587/610), which is a reporter present in the AIO-mCherry plasmid. FACS was done in a (BD FACSAria) III Cell Sorter (Becton Dickinson). After 8 days post-sorting, gDNA was extracted for high-fidelity PCR using specific primers for on- and off-target sequences (Table S3). An *in silico* PCR was done to determine the theoretical amplicon sizes using online software from the Genomic Institute of the University of California, Santa Cruz (https://genome.ucsc.edu/cgi-bin/hgPcr). PCR products were then sequenced by Sanger using the same primer for PCR amplification. Electropherograms were used to detect sequence changes by trace decomposition through ICE Analysis from Synthego v2.0.[73]

Homologous recombination assays

NIH/3T3 cells were transfected with Donor ROSA26:GALNS and CRISPR-Cas9 plasmids for 12 h. Then, gDNA was isolated, and a PCR was conducted using a forward primer flanking the bGH sequence placed in the Donor ROSA26:GALNS and a reverse primer flanking a genomic ROSA26 region absent in the homologous recombination right arm of the donor ROSA26:GALNS (Table S3). The resulting PCR product was sequenced by Sanger.

IONPs characterization

IONPs were purchased from OZ Biosciences in a formulation denominated *in vivo* DogtorMag, composed of magnetite (Fe_3O_4) and lipid-based nanoparticles positively charged. Plasmid loading was performed according to the manufacturer's instructions. To determine the maximum pDNA loading capacity of these IONPs, ratios

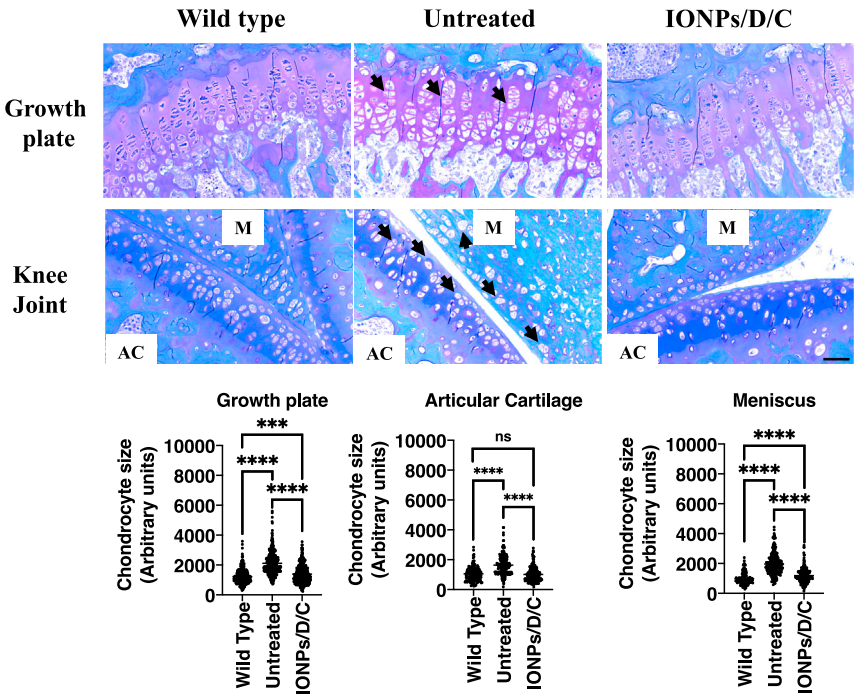

Figure 7. Knee joint pathology analysis in MTOL mice

(Top) Representative microphotography of the growth plate (tibia) and knee joint (meniscus [M] and articular cartilage [AC]) from WT (n = 3), untreated (n = 3), and IONPs/donor/CRISPR (IONPs/D/C) (n = 5) treated MTOL mice. (Bottom) Mean chondrocyte size average from chondrocytes in the growth plate (n = 342 cells), meniscus (n = 224 cells), and AC (n = 254 cells) for each experimental group. Each dot represents a chondrocyte. Original magnification ×40. ***p ≤ 0.001, ****p ≤ 0.0001. Kruskal-Wallis test.

ranging from 1:1 to 1:10 were tested. After IONPs loading, 5 μL loading buffer (New England Biolabs) was added, and 15 μL were loaded on 1% w/v agarose gel stained with GelRed Nucleic Acid stain (Sigma-Aldrich) and resolved at 100 V for 90 min. Images were acquired using a FluorChem E instrument (Bio-Techne) and processed with ImageJ software version 1.53t (NIH). These experiments revealed a maximum ratio of 1:1.5 IONPs:pDNA (Figure S5), which agreed with those reported by Park et al., 2022.[43] IONPs:pDNA complexes were further assessed to hydrodynamic diameter and Z potential using dynamic light scattering in a Zeta-Sizer Nano-ZS (Malvern Panalytical).

DpnI *restriction assay*

To test if IONPs protect the loaded pDNA against endonucleases-mediated digestion, a *Dpn*I digestion was carried out according to previous protocols.[27] Briefly, IONPs carrying pDNA in a ratio 1:1.5 IONPs:pDNA in glucose 5% were incubated with 20 U *Dpn*I for 1 h at 37°C. Then, 8 μL loading buffer (New England Biolabs) was added, and the whole reaction volume was resolved at 100 V for 90 min. Images were acquired and processed as detailed previously.

In vitro characterization of the IONPs-coupled CRISPR-nCas9 system in MTOL fibroblasts

Long-term editing in MTOL fibroblasts

Long-term CRISPR-nCas9-based genome editing was performed in MTOL fibroblasts by transfecting them with CRISPR-nCas9 and donor ROSA26:GALNS plasmids using both LP-LTX (Invitrogen) and IONPs, according to manufacturer's instructions. Briefly, 40,000 cells/mL MTOL fibroblasts were seeded on 24-well plates (Falcon) 24 h before assays. The media was removed and replaced by a fresh one 1 h before transfection. MTOL fibroblasts were transfected with 0.5 μg CRISPR-nCas9 and 0.5 μg donor plasmids. For IONPs, the plates were placed on a magnetic plate (DogtorMag) for 30 min at room temperature (RT), following the manufacturer's recommendations. The media was replaced by fresh ones after 24 and 48 h post-transfection with IONPs and LP-LTX, respectively, and followed up to 1 month. Culture media was changed every four days and stored at −20°C until its use in the GALNS assessment.

GALNS activity assays

Intra- and extracellular GALNS activity was measured using 4-MU-Gal-6S at 22 mM (Toronto Chemicals Research) according to previous protocols.[31,74] Briefly, 2 μL of the sample was incubated with 9 μL 4-MU-Gal-6S and 19 μL Milli-Q ultrapure water (Sigma). Samples were incubated for 17 h and then set with 2 μL β-galactosidase (10 mg/mL, Sigma-Aldrich) for 1 h. The reaction was stopped by adding 968 μL glycine-carbonate pH 9.8 buffer. Then, 200 μL were transferred to 96-well black flat-bottom microplates (Corning). Finally, samples were read in a FLUOstar Omega microplate reader (*Exc/Emi*: 365/450 nm, BMG LabTech). One unit of enzyme activity (U) was defined as the amount of enzyme hydrolyzing of 1 nmol substrate per hour. The standard curve was done with 4-methylumbelliferone (Sigma). Specific enzyme activity was expressed as units per milligram protein, which was determined using a BCA Protein Assay Kit (Thermo Fisher Scientific).

Lysosomal mass determination

One month after treatment, MTOL fibroblasts were stained with LysoTracker Deep Red (*Exc/Emi*: 647/668 nm; Thermo Fisher Scientific) according to the previous protocols.[31,75] Briefly, the fibroblasts were incubated for 1 h with 50 nM diluted in supplemented DMEM for flow cytometry experiments. The fibroblasts were harvested by trypsinization for flow cytometry experiments and washed twice with 1× PBS. Finally, the fibroblasts were homogenized in 1 X Hanks' Balanced Salt solution plus 2% FBS. We recorded 50,000

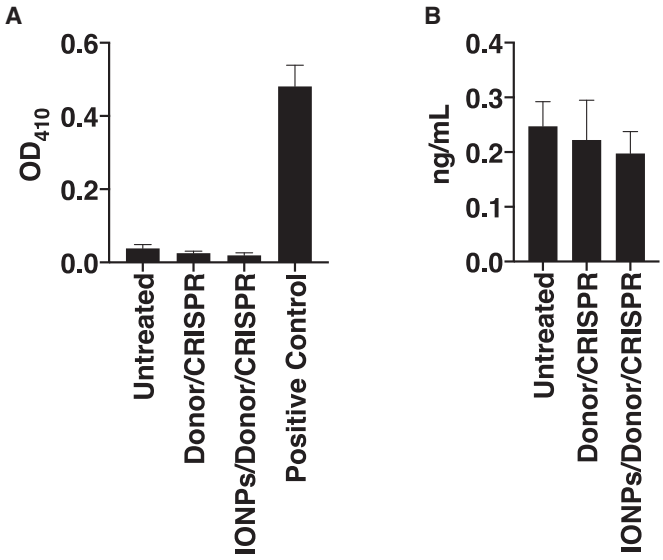

Figure 8. Antibodies-mediated immune response in MTOL mice

(A) Anti-GALNS antibodies response. Positive control corresponds with samples from MPS IVA mice (MKC strain) under ERT. (B) Anti-nCas9 antibodies response in plasma samples from untreated (n = 5), donor/CRISPR (n = 3), and IONPs/Donor/CRISPR (n = 5) groups.

ungated events in the NovoCyte 3000 cytometer (Agilent Technologies). Propidium iodide was used for identifying viable fibroblasts. Viable single cells were analyzed in the FlowJo software.

For epifluorescence microscopy, the fibroblasts, seeded on Poly-D lysine-covered coverslips, were incubated for 1 h with 70 nM LysoTracker diluted in supplemented DMEM. The cells were washed once with 1× PBS and fixed with 4% paraformaldehyde in PBS (4% PFA) at RT for 15 min. Three washes with 1× PBS were done and then transferred to slides containing a drop of Prolong Glass Antifade Mountant with NucBlue Stain (Thermo Fisher). Finally, the MTOL fibroblasts were observed under fluorescence microscopy (Axio Observer Z1 microscope, Zeiss). The images were analyzed with the aid of the ImageJ software version 1.53t (NIH).[76]

In vivo *assessment of the IONPs-coupled CRISPR-nCas9 system in MTOL mice MPS IVA mice model*

Previously, we developed an MPS IVA mice tolerant to human GALN protein (MTOL, *GALNS*$^{tm(hC79S.mC76S)slu}$) in the C57BL/6 background.[32] MTOL mice contain a transgene expressing mutant hGALNS (GALNS^{hC79S}) in intron 1 of the mouse genome and an active site mutation in mouse GALNS (GALNS^{mC76S}) adjacent to exon 2. At birth, homozygotes MTOL male mice were injected into the superficial temporal vein with 2.5 μg IONPs carrying 4 μg CRISPR-nCas9-related plasmids. Untreated MTOL and unaffected C57BL/6 littermates were injected with glucose 5% and included as controls. A total of 100 μL were injected into each experimental group. The dose was determined after dose-response experiments in which IONPs: CRISPR-nCas9 doses ranging between 0 and 20 μg were evaluated (Figure S6). Treated and control animals were weaned for 21 days and raised independently. Mice were euthanized at 12 weeks post-treatment with CO_2 gas. All animal care and experiments were approved by the Research and Ethics Committee of the Faculty of Science at Pontificia Universidad Javeriana (InvestigarPUJ 20289) and the Institutional Animal Care and Use Committee of Nemours Children's Health (Protocol ID: RSP21-12482-002).

Ex vivo *biodistribution analysis*

To determine the biodistribution of the IONPs carrying the CRISPR-nCas9 system, an *ex vivo* analysis was performed according to the protocol described by Park et al.[43] Briefly, 20 μg loaded IONPs were fluorescently labeled with DiIC18(5) solid (1,1′-dioctadecyl-3,3,3′,3′-tetramethylindodicarbocyanine, 4-chlorobenzenesulfonate Salt) (ThermoFisher Scientific) for 10 min at RT. Then, IONPs were washed three times in an amicon Ultra-0.5 10K centrifugal device (DID, UFC501008, Millipore) with glucose 5%. DiIC-labeled IONPs were injected into 8-week-old animals via tail injection. Unlabeled IONPs were injected in mice as autofluorescence control. One hour later, the animals were euthanized and autopsied with CO_2. Tissues were collected and visualized in an IVIS Lumina LT Series instrument using a Cy5 filter (*Exc/Emi*, 644/665 nm), and images were processed with Aura Imaging software (https://www.spectralinvivo.com/imaging/software).

Blood and tissue collection

Blood samples were collected biweekly in EDTA-containing tubes (BD Microtainer) by a venous puncture on the superficial temporal vein with a 22G needle (BD Eclipse Vacutainer), starting at 4 weeks post-injection. At the endpoint, blood was collected in EDTA and non-anticoagulant tubes (BD MicrotainerUSA) to obtain plasma and serum, respectively. Plasma samples were stored at −20°C, while serum samples were stored at −80°C until their processing. Additionally, at autopsy, transcardiac perfusion with NaCl 0.9% w/v was performed with a Masterflex L/S Easy-Load II system (Wavantor) using a 27G X $^{3}/_{4}$ scalp vein into the left ventricle. Then, the arms, brain, eyes, gonads, heart, kidneys, legs, liver, lungs, muscle, spine, spleen, and trachea were collected and preserved at −80°C or in PFA 4% accordingly.

IONPs-coupled CRISPR-Cas9-related toxicity

To determine the potential side effect of the IONPs empty or carrying the CRISPR-nCas9 system, alanine transaminase (EALT-100, BioAssay Systems), aspartate transaminase (EASTR-100, BioAssay Systems), blood urea (DIUR-100), blood urea nitrogen (calculated from urea values), and plasma creatinine (700460, Cayman Chemical), according with manufacturer's instructions. Besides, serum iron (702230, Cayman Chemical), total iron-binding capacity (TIBC, 702230, Cayman Chemical), and percentage of saturation of transferrin (calculated from serum iron and TIBC) were conducted. All the reactions were performed on 96-well plates and read in a FLUOstar Omega microplate reader BMG LabTech) at the wavelength specified by the supplier.

GALNS activity

GALNS activity was measured on plasma samples following the protocol described for *in vitro* validation. For tissue samples, ~50 mg of each tissue was transferred to homogenizer tubes (OMNI International) containing Tris buffer (25 mM, 1 mM PMSF, pH 7.2), and homogenized in a Bead Mill Homogenizer (OMNI International). The homogenized tissues were used for GALNS activity as described for *in vitro* validation.

Mono-KS levels

Plasma, liver, and humerus samples were analyzed for KS by liquid chromatography-tandem mass spectrometry (LC-MS/MS) as described previously.[17] Disaccharides were isolated by digestion with chondroitinase B, heparitinase, and keratanase II. Samples were run in a 1290 Infinity LC system with a 6460 triple quad mass spectrometer (Agilent Technologies). Tissue homogenization and disaccharide analysis were performed as described in Methodology S1.

Hematoxylin and eosin staining

Liver and kidneys from treated MTOL mice were stained with hematoxylin and eosin. PFA-fixed samples were xylene clearing, paraffin embedding, and microtome cutting into 6-mm-thick sections. Tissues were analyzed under light microscopy to determine liver and kidney injury.

Toluidine blue staining

Cellular vacuolation was determined in 4% PFA preserved samples through toluidine blue staining in the knee joint to evaluate cell vacuolation as described previously.[10] Briefly, the knee joint was decalcified for three weeks in a decalcification solution containing 10% EDTA in 0.1 M Tris HCl buffer (pH 7.0). The decalcification solution was changed twice per week by a fresh one. Then, samples were washed three times with 0.1 M sodium cacodylate buffer and later fixed for 2 h in 1% osmium tetroxide in 0.1 M sodium cacodylate buffer. Sample dehydration was performed by keeping samples on ascending ethanol solutions (25%–95%). An initial infiltration was done by incubating samples into 1 part 100% anhydrous ethanol:1 part propylene oxide for 1 h, followed by immersion in 100% for one additional hour. Samples were then embedded in Spur low viscosity resin (EMS) and polymerized at 60°C for 2 days. Finally, embedded blocks were sectioned to obtain 0.5-μL-thick sections with a Leica UC7 ultramicrotome instrument (Leica Biosystems) and then stained using toluidine blue (EMS). Images were acquired using an Olympus BX51 light microscopy and processed with ImageJ software version 1.53t (NIH).[76]

Anti-GALNS antibodies

To evaluate the anti-GALNS antibody response upon CRISPR-nCas9 treatment, plasma samples were used for ELISA experiments, according to the protocol reported by Sawamoto et al.[17] Briefly, 100 μL 2 μg/mL elosulfase alfa (Vimizin, Biomarin Pharmaceutical Inc.) in 15 mM Na_2CO_3, 35 mM $NaHCO_3$, and 0.02% NaN_3, pH 9.6 were seeded on 96-well plates (Falcon) and incubate overnight at 4°C in a wet chamber. The next day, the wells were washed three times with 250 μL Tris-buffered saline (TBS)-T (10 mM Tris pH 7.5, 150 mM NaCl, 0.05% Tween 20) and wells were blocked by adding 200 μL 3% BSA in 1× PBS pH 7.2. The plate was then incubated for 1 h at room temperature, and later washes were done with 250 μL TBS-T. Diluted plasma samples (1:100 in TBS-T) were added in duplicate and incubated for 2.5 h at 37°C.

The plate was washed four times with 250 μL TBS-T, and 100 μL peroxidase-conjugated goat anti-mouse immunoglobulin G (HRP-IgG 1:1000 in TBS-T) was included. An additional incubation at RT was done for 1 h, and the plate was washed three times with 250 μL TBS-T and twice with 250 μL TBS. Finally, 100 μL peroxidase substrate (ABTS, Invitrogen, Thermo Fisher Scientific) was added and incubated for 30 min at RT. The reaction was stopped by adding 100 μL 1% SDS, and the plate was then read at 410 nm in a FLUOstar Omega microplate reader (BMG LabTech). Data were analyzed as optical density at 410 nm. Plasma samples from MKC mice under ERT with elosulfase alfa (Vimizin) were included as a positive control.

Anti-nCas9 antibodies

To evaluate the anti-nCas9 antibody response after CRISPR-nCas9 treatment, a protocol was standardized according to procedures reported by Chew et al.,[77] Simhadri et al.,[66] Charlesworth et al.,[78] and Sawamoto et al.[17] Briefly, A 96-well plate (Falcon) was covered with 100 μg/well purified nCas9 protein (CAS9-D10A, Millipore) in 15 mM Na_2CO_3, 35 mM $NaHCO_3$, and 0.02% NaN_3, pH 9.6. After overnight incubation at 4°C, three washes were done using TBS-T, and then the plate was blocked using 3% BSA in 1× PBS pH 7.2 for 1 h at RT. Three washes were performed with TBS-T and then incubated with 100 μL mouse plasma (1:100 in TBS-T) or primary antibody dilutions (sc-517386) in duplicate. The following steps were performed as detailed for anti-GALNS antibodies. Anti-nCas9 antibodies were reported as ng/mL after comparing the OD obtained for each sample against a standard curve (Figure S7).

Vector copy number assays

Liver and testes were used to determine the presence of Donor ROSA26:GALNS and nCas9 after long-term assessment in MTOL mice using digital PCR in a QuantStudio 3D digital real-time PCR system (Thermo Fisher Scientific). The *Tfrc* gene was used as a mouse genome reference and detected through a TaqMan probe (4458367), while an EGFP TaqMan probe (Mr00660654) targeting the donor template and a customized TaqMan probe for nCas9 (57085_CDPRK2P).

Statistical analysis

Experimental data were analyzed using GraphPad Prism version 8.0.0 for Mac (GraphPad SoftwareUSA) and the statistical software R (version 4.3.0; R Core Team, R Foundation for Statistical Computing). The data are presented as mean ± standard error (SE). Shapiro-Wilk and Levene's tests were used to evaluate the normal distribution and homoscedasticity. Mean comparison between groups was made with Student's *t*-test, Mann-Whitney U test, or ANOVA,

according to the normality test findings; $p < 0.05$ was considered statistically significant.

DATA AND CODE AVAILABILITY

Data supporting the findings of this work are available within the paper and its Supplemental Information files.

SUPPLEMENTAL INFORMATION

Supplemental information can be found online at https://doi.org/10.1016/j.omtm.2023.101153.

ACKNOWLEDGMENTS

A.F.L. received a PhD scholarship from Pontificia Universidad Javeriana. C.J.A.D was supported by Pontificia Universidad Javeriana (Investigar PUJ 20386, 20567, and 20646), Ministry of Science, Technology, and Innovation from Colombia (Contract 120380763212, ID 8352, and CT-499-2021, ID 9630), and the National MPS Society (ID 9507). This work was also supported by grants from the Austrian MPS society, A Cure for Robert, Inc., The Carol Ann Foundation, Angelo R. Cali & Mary V. Couch Family Foundation, Inc., The Vain and Hyde Family Foundation, Inc., The Bennett Foundation, Jacob Randall Foundation, and Nemours Funds. S.T. was supported by an Institutional Development Award from the Eunice Kennedy Shriver National Institute of Child Health & Human Development of the National Institutes of Health (NICHD) (1R01HD10254501A1).

AUTHOR CONTRIBUTIONS

A.F.L. and C.J.A.D. conceived the project; A.F.L. performed most experiments, analyzed primary data, and wrote the manuscript; B.C. aided during *in vivo* injections and autopsies; N.F. performed tissue processing for pathology analysis; K.S. performed LC-MS/MS analysis of GAGs; S.T. provided permanent direction during *in vivo* assessment, data analysis, and manuscript preparation.

DECLARATION OF INTERESTS

The authors declare no conflict of interest.

REFERENCES

1. Zanetti, A., D'Avanzo, F., AlSayed, M., Brusius-Facchin, A.C., Chien, Y.H., Giugliani, R., Izzo, E., Kasper, D.C., Lin, H.Y., Lin, S.P., et al. (2021). Molecular basis of mucopolysaccharidosis IVA (Morquio A syndrome): A review and classification of GALNS gene variants and reporting of 68 novel variants. Hum. Mutat. *42*, 1384–1398.
2. Sawamoto, K., Álvarez González, J.V., Piechnik, M., Otero, F.J., Couce, M.L., Suzuki, Y., and Tomatsu, S. (2020). Mucopolysaccharidosis IVA: Diagnosis, Treatment, and Management. Int. J. Mol. Sci. *21*, 1517.
3. Cleary, M., Davison, J., Gould, R., Geberhiwot, T., Hughes, D., Mercer, J., Morrison, A., Murphy, E., Santra, S., Jarrett, J., et al. (2021). Impact of long-term elosulfase alfa treatment on clinical and patient-reported outcomes in patients with mucopolysaccharidosis type IVA: results from a Managed Access Agreement in England. Orphanet J. Rare Dis. *16*, 38.
4. Stevens, B., Kenny, T., Thomas, S., Morrison, A., Jarrett, J., and Jain, M. (2021). Elosulfase alfa in the treatment of mucopolysaccharidosis type IVA: insights from the first managed access agreement. Orphanet J. Rare Dis. *16*, 394.
5. Hendriksz, C.J., Burton, B., Fleming, T.R., Harmatz, P., Hughes, D., Jones, S.A., Lin, S.P., Mengel, E., Scarpa, M., Valayannopoulos, V., et al. (2014). Efficacy and safety of enzyme replacement therapy with BMN 110 (elosulfase alfa) for Morquio A syndrome (mucopolysaccharidosis IVA): a phase 3 randomised placebo-controlled study. J. Inherit. Metab. Dis. *37*, 979–990.
6. Concolino, D., Deodato, F., and Parini, R. (2018). Enzyme replacement therapy: efficacy and limitations. Ital. J. Pediatr. *44*, 120.
7. Donida, B., Marchetti, D.P., Biancini, G.B., Deon, M., Manini, P.R., da Rosa, H.T., Moura, D.J., Saffi, J., Bender, F., Burin, M.G., et al. (2015). Oxidative stress and inflammation in mucopolysaccharidosis type IVA patients treated with enzyme replacement therapy. Biochim. Biophys. Acta *1852*, 1012–1019.
8. Tomatsu, S., Sawamoto, K., Shimada, T., Bober, M.B., Kubaski, F., Yasuda, E., Mason, R.W., Khan, S., Alméciga-Díaz, C.J., Barrera, L.A., et al. (2015). Enzyme replacement therapy for treating mucopolysaccharidosis type IVA (Morquio A syndrome): effect and limitations. Expert Opin. Orphan Drugs *3*, 1279–1290.
9. Chen, H.H., Sawamoto, K., Mason, R.W., Kobayashi, H., Yamaguchi, S., Suzuki, Y., Orii, K., Orii, T., and Tomatsu, S. (2019). Enzyme replacement therapy for mucopolysaccharidoses; past, present, and future. J. Hum. Genet. *64*, 1153–1171.
10. Taylor, M., Khan, S., Stapleton, M., Wang, J., Chen, J., Wynn, R., Yabe, H., Chinen, Y., Boelens, J.J., Mason, R.W., et al. (2019). Hematopoietic Stem Cell Transplantation for Mucopolysaccharidoses: Past, Present, and Future. Biol. Blood Marrow Transplant. *25*, e226–e246.
11. Sawamoto, K., and Tomatsu, S. (2019). Development of Substrate Degradation Enzyme Therapy for Mucopolysaccharidosis IVA Murine Model. Int. J. Mol. Sci. *20*, 4139.
12. Olarte-Avellaneda, S., Cepeda Del Castillo, J., Rojas-Rodriguez, A.F., Sánchez, O., Rodríguez-López, A., Suárez García, D.A., Pulido, L.M.S., and Alméciga-Díaz, C.J. (2020). Bromocriptine as a Novel Pharmacological Chaperone for Mucopolysaccharidosis IV A. ACS Med. Chem. Lett. *11*, 1377–1385.
13. Alméciga-Diaz, C.J., Hidalgo, O.A., Olarte-Avellaneda, S., Rodríguez-López, A., Guzman, E., Garzón, R., Pimentel-Vera, L.N., Puentes-Tellez, M.A., Rojas-Rodriguez, A.F., Gorshkov, K., et al. (2019). Identification of Ezetimibe and Pranlukast as Pharmacological Chaperones for the Treatment of the Rare Disease Mucopolysaccharidosis Type IVA. J. Med. Chem. *62*, 6175–6189.
14. Leal, A.F., Benincore-Flórez, E., Rintz, E., Herreño-Pachón, A.M., Celik, B., Ago, Y., Alméciga-Díaz, C.J., and Tomatsu, S. (2023). Mucopolysaccharidoses: Cellular Consequences of Glycosaminoglycans Accumulation and Potential Targets. Int. J. Mol. Sci. *24*, 1–21.
15. Leal, A.F., Espejo-Mojica, A.J., Sánchez, O.F., Ramírez, C.M., Reyes, L.H., Cruz, J.C., and Alméciga-Díaz, C.J. (2020). Lysosomal storage diseases: current therapies and future alternatives. J. Mol. Med. *98*, 931–946.
16. Sawamoto, K., Chen, H.H., Alméciga-Díaz, C.J., Mason, R.W., and Tomatsu, S. (2018). Gene therapy for Mucopolysaccharidoses. Mol. Genet. Metabol. *123*, 59–68.
17. Sawamoto, K., Karumuthil-Melethil, S., Khan, S., Stapleton, M., Bruder, J.T., Danos, O., and Tomatsu, S. (2020). Liver-Targeted AAV8 Gene Therapy Ameliorates Skeletal and Cardiovascular Pathology in a Mucopolysaccharidosis IVA Murine Model. Mol. Ther. Methods Clin. Dev. *18*, 50–61.
18. Alméciga-Díaz, C.J., Montaño, A.M., Barrera, L.A., and Tomatsu, S. (2018). Tailoring the AAV2 capsid vector for bone-targeting. Pediatr. Res. *84*, 545–551.
19. Puentes-Tellez, M.A., Sánchez, O.F., Rojas-Rodriguez, F., Benincore-Flórez, E., Barbosa, H., and Alméciga Díaz, C.J. (2021). Evaluation of HIV-1 derived lentiviral vectors as transductors of Mucopolysaccharidosis type IV a fibroblasts. Gene *780*, 145527.
20. Bertolin, J., Sánchez, V., Ribera, A., Jaén, M.L., Garcia, M., Pujol, A., Sánchez, X., Muñoz, S., Marcó, S., Pérez, J., et al. (2021). Treatment of skeletal and non-skeletal alterations of Mucopolysaccharidosis type IVA by AAV-mediated gene therapy. Nat. Commun. *12*, 5343.
21. Zhao, Z., Anselmo, A.C., and Mitragotri, S. (2022). Viral vector-based gene therapies in the clinic. Bioeng. Transl. Med. *7*, e10258.
22. Wang, J.Y., and Doudna, J.A. (2023). CRISPR technology: A decade of genome editing is only the beginning. Science *379*, eadd8643.
23. Leal, A.F., Fnu, N., Benincore-Flórez, E., Herreño-Pachón, A.M., Echeverri-Peña, O.Y., Alméciga-Díaz, C.J., and Tomatsu, S. (2023). The landscape of CRISPR/Cas9 for inborn errors of metabolism. Mol. Genet. Metabol. *138*, 106968.

24. Batool, A., Malik, F., and Andrabi, K.I. (2021). Expansion of the CRISPR/Cas Genome-Sculpting Toolbox: Innovations, Applications and Challenges. Mol. Diagn. Ther. *25*, 41–57.

25. Robbins, G.M., Wang, M., Pomeroy, E.J., and Moriarity, B.S. (2021). Nonviral genome engineering of natural killer cells. Stem Cell Res. Ther. *12*, 350.

26. Scharenberg, S.G., Poletto, E., Lucot, K.L., Colella, P., Sheikali, A., Montine, T.J., Porteus, M.H., and Gomez-Ospina, N. (2020). Engineering monocyte/macrophage-specific glucocerebrosidase expression in human hematopoietic stem cells using genome editing. Nat. Commun. *11*, 3327.

27. Leal, A.F., Cifuentes, J., Quezada, V., Benincore-Flórez, E., Cruz, J.C., Reyes, L.H., Espejo-Mojica, A.J., and Alméciga-Díaz, C.J. (2022). CRISPR/nCas9-Based Genome Editing on GM2 Gangliosidoses Fibroblasts via Non-Viral Vectors. Int. J. Mol. Sci. *23*, 10672.

28. Ou, L., Przybilla, M.J., Tăbăran, A.F., Overn, P., O'Sullivan, M.G., Jiang, X., Sidhu, R., Kell, P.J., Ory, D.S., and Whitley, C.B. (2020). A novel gene editing system to treat both Tay-Sachs and Sandhoff diseases. Gene Ther. *27*, 226–236.

29. Hong, S.A., Seo, J.H., Wi, S., Jung, E.S., Yu, J., Hwang, G.H., Yu, J.H., Baek, A., Park, S., Bae, S., and Cho, S.R. (2022). In vivo gene editing via homology-independent targeted integration for adrenoleukodystrophy treatment. Mol. Ther. *30*, 119–129.

30. Schuh, R.S., Gonzalez, E.A., Tavares, A.M.V., Seolin, B.G., Elias, L.d.S., Vera, L.N.P., Kubaski, F., Poletto, E., Giugliani, R., Teixeira, H.F., et al. (2020). Neonatal nonviral gene editing with the CRISPR/Cas9 system improves some cardiovascular, respiratory, and bone disease features of the mucopolysaccharidosis I phenotype in mice. Gene Ther. *27*, 74–84.

31. Leal, A.F., and Alméciga-Díaz, C.J. (2022). Efficient CRISPR/Cas9 nickase-mediated genome editing in an in vitro model of mucopolysaccharidosis IVA. Gene Ther. *1–8*.

32. Tomatsu, S., Gutierrez, M., Nishioka, T., Yamada, M., Yamada, M., Tosaka, Y., Montaño, A.M., Montaño, A.M., Vieira, M.B., Peña, O.M., et al. (2005). Development of MPS IVA mouse (Galnstm(hC79S.mC76S)slu) tolerant to human N-acetylgalactosamine-6-sulfate sulfatase. Hum. Mol. Genet. *14*, 3321–3335.

33. Rintz, E., Herreño-Pachón, A.M., Celik, B., Nidhi, F., Khan, S., Benincore-Flórez, E., and Tomatsu, S. (2023). Bone Growth Induction in Mucopolysaccharidosis IVA Mouse. Int. J. Mol. Sci. *24*, 9890.

34. Asmamaw, M., and Zawdie, B. (2021). Mechanism and Applications of CRISPR/Cas-9-Mediated Genome Editing. Biologics *15*, 353–361.

35. Cui, Y., Xu, J., Cheng, M., Liao, X., and Peng, S. (2018). Review of CRISPR/Cas9 sgRNA Design Tools. Interdiscip. Sci. *10*, 455–465.

36. Uniyal, A.P., Mansotra, K., Yadav, S.K., and Kumar, V. (2019). An overview of designing and selection of sgRNAs for precise genome editing by the CRISPR-Cas9 system in plants. 3 Biotech *9*, 223.

37. Zhang, J., Zhang, T., and Gao, J. (2022). Biocompatible Iron Oxide Nanoparticles for Targeted Cancer Gene Therapy: A Review. Nanomaterials *12*, 3323.

38. Dadfar, S.M., Camozzi, D., Darguzyte, M., Roemhild, K., Varvarà, P., Metselaar, J., Banala, S., Straub, M., Güvener, N., Engelmann, U., et al. (2020). Size-isolation of superparamagnetic iron oxide nanoparticles improves MRI, MPI and hyperthermia performance. J. Nanobiotechnol. *18*, 22.

39. Dadfar, S.M., Roemhild, K., Drude, N.I., von Stillfried, S., Knüchel, R., Kiessling, F., and Lammers, T. (2019). Iron oxide nanoparticles: Diagnostic, therapeutic and theranostic applications. Adv. Drug Deliv. Rev. *138*, 302–325.

40. Wei, H., Hu, Y., Wang, J., Gao, X., Qian, X., and Tang, M. (2021). Superparamagnetic Iron Oxide Nanoparticles: Cytotoxicity, Metabolism, and Cellular Behavior in Biomedicine Applications. Int. J. Nanomed. *16*, 6097–6113.

41. Portilla, Y., Mellid, S., Paradela, A., Ramos-Fernández, A., Daviu, N., Sanz-Ortega, L., Pérez-Yagüe, S., Morales, M.P., and Barber, D.F. (2021). Iron Oxide Nanoparticle Coatings Dictate Cell Outcomes Despite the Influence of Protein Coronas. ACS Appl. Mater. Interfaces *13*, 7924–7944.

42. Alphandéry, E. (2019). Biodistribution and targeting properties of iron oxide nanoparticles for treatments of cancer and iron anemia disease. Nanotoxicology *13*, 573–596.

43. Park, H., Kim, D., Cho, B., Byun, J., Kim, Y.S., Ahn, Y., Hur, J., Oh, Y.K., and Kim, J. (2022). In vivo therapeutic genome editing via CRISPR/Cas9 magnetoplexes for myocardial infarction. Biomaterials *281*, 121327.

44. Arami, H., Khandhar, A., Liggitt, D., and Krishnan, K.M. (2015). In vivo delivery, pharmacokinetics, biodistribution and toxicity of iron oxide nanoparticles. Chem. Soc. Rev. *44*, 8576–8607.

45. Jokerst, J.V., Lobovkina, T., Zare, R.N., and Gambhir, S.S. (2011). Nanoparticle PEGylation for imaging and therapy. Nanomedicine (Lond) *6*, 715–728.

46. Salimi, M., Sarkar, S., Fathi, S., Alizadeh, A.M., Saber, R., Moradi, F., and Delavari, H. (2018). Biodistribution, pharmacokinetics, and toxicity of dendrimer-coated iron oxide nanoparticles in BALB/c mice. Int. J. Nanomed. *13*, 1483–1493.

47. Yu, Q., Xiong, X.Q., Zhao, L., Xu, T.T., Bi, H., Fu, R., and Wang, Q.H. (2018). Biodistribution and Toxicity Assessment of Superparamagnetic Iron Oxide Nanoparticles In Vitro and In Vivo. Curr. Med. Sci. *38*, 1096–1102.

48. Poletto, E., Silva, A.O., Weinlich, R., Martin, P.K.M., Torres, D.C., Giugliani, R., and Baldo, G. (2023). Gene therapy for lysosomal storage disorders: future perspectives. Expert Opin Biol Ther *23*, 353–364.

49. Wood, S.R., and Bigger, B.W. (2022). Delivering gene therapy for mucopolysaccharide diseases. Front. Mol. Biosci. *9*, 965089.

50. Tomatsu, S., Azario, I., Sawamoto, K., Pievani, A.S., Biondi, A., and Serafini, M. (2016). Neonatal cellular and gene therapies for mucopolysaccharidoses: the earlier the better? J. Inherit. Metab. Dis. *39*, 189–202.

51. Morrone, A., Tylee, K.L., Al-Sayed, M., Brusius-Facchin, A.C., Caciotti, A., Church, H.J., Coll, M.J., Davidson, K., Fietz, M.J., Gort, L., et al. (2014). Molecular testing of 163 patients with Morquio A (Mucopolysaccharidosis IVA) identifies 39 novel GALNS mutations. Mol. Genet. Metabol. *112*, 160–170.

52. Filocamo, M., Tomanin, R., Bertola, F., and Morrone, A. (2018). Biochemical and molecular analysis in mucopolysaccharidoses: what a paediatrician must know. Ital. J. Pediatr. *44*, 129.

53. Selvam, P., Jain, A., Abbott, J., Ahuja, A.S., Cheema, A., Bruno, K.A., Atwal, H., Forghani, I., Caulfield, T., and Atwal, P.S. (2022). Molecular Modeling and Phenotypic Description of a Patient with a Novel Exonic Deletion of *GALNS* with Resultant Morquio Syndrome with Two Successful Pregnancies. Mol. Syndromol. *13*, 282–289.

54. Sukegawa, K., Nakamura, H., Kato, Z., Tomatsu, S., Montaño, A.M., Fukao, T., Toietta, G., Tortora, P., Orii, T., and Kondo, N. (2000). Biochemical and structural analysis of missense mutations in N-acetylgalactosamine-6-sulfate sulfatase causing mucopolysaccharidosis IVA phenotypes. Hum. Mol. Genet. *9*, 1283–1290.

55. Weber, T. (2021). Anti-AAV Antibodies in AAV Gene Therapy: Current Challenges and Possible Solutions. Front. Immunol. *12*, 658399.

56. Ertl, H.C.J. (2022). Immunogenicity and toxicity of AAV gene therapy. Front. Immunol. *13*, 975803.

57. Prasad, S., Dimmock, D.P., Greenberg, B., Walia, J.S., Sadhu, C., Tavakkoli, F., and Lipshutz, G.S. (2022). Immune Responses and Immunosuppressive Strategies for Adeno-Associated Virus-Based Gene Therapy for Treatment of Central Nervous System Disorders: Current Knowledge and Approaches. Hum. Gene Ther. *33*, 1228–1245.

58. Long, B.R., Veron, P., Kuranda, K., Hardet, R., Mitchell, N., Hayes, G.M., Wong, W.Y., Lau, K., Li, M., Hock, M.B., et al. (2021). Early Phase Clinical Immunogenicity of Valoctocogene Roxaparvovec, an AAV5-Mediated Gene Therapy for Hemophilia A. Mol. Ther. *29*, 597–610.

59. Nathwani, A.C., Reiss, U.M., Tuddenham, E.G.D., Rosales, C., Chowdary, P., McIntosh, J., Della Peruta, M., Lheriteau, E., Patel, N., Raj, D., et al. (2014). Long-term safety and efficacy of factor IX gene therapy in hemophilia B. N. Engl. J. Med. *371*, 1994–2004.

60. Lek, A., Wong, B., Keeler, A., Blackwood, M., Ma, K., Huang, S., Sylvia, K., Batista, A.R., Artinian, R., Kokoski, D., et al. (2023). Death after High-Dose rAAV9 Gene Therapy in a Patient with Duchenne's Muscular Dystrophy. N. Engl. J. Med. *389*, 1203–1210.

61. Gomez-Ospina, N., Scharenberg, S.G., Mostrel, N., Bak, R.O., Mantri, S., Quadros, R.M., Gurumurthy, C.B., Lee, C., Bao, G., Suarez, C.J., et al. (2019). Human genome-edited hematopoietic stem cells phenotypically correct Mucopolysaccharidosis type I. Nat. Commun. *10*, 4045.

62. Cheng, H., Zheng, Z., and Cheng, T. (2020). New paradigms on hematopoietic stem cell differentiation. Protein Cell *11*, 34–44.

63. Höfer, T., and Rodewald, H.R. (2018). Differentiation-based model of hematopoietic stem cell functions and lineage pathways. Blood *132*, 1106–1113.

64. Mehta, A., and Merkel, O.M. (2020). Immunogenicity of Cas9 Protein. J. Pharmaceut. Sci. *109*, 62–67.

65. Crudele, J.M., and Chamberlain, J.S. (2018). Cas9 immunity creates challenges for CRISPR gene editing therapies. Nat. Commun. *9*, 3497.

66. Simhadri, V.L., McGill, J., McMahon, S., Wang, J., Jiang, H., and Sauna, Z.E. (2018). Prevalence of Pre-existing Antibodies to CRISPR-Associated Nuclease Cas9 in the USA Population. Mol. Ther. Methods Clin. Dev. *10*, 105–112.

67. Wiesinger, A.M., Bigger, B., Giugliani, R., Scarpa, M., Moser, T., Lampe, C., Kampmann, C., and Lagler, F.B. (2022). The Inflammation in the Cytopathology of Patients With Mucopolysaccharidoses- Immunomodulatory Drugs as an Approach to Therapy. Front. Pharmacol. *13*, 863667.

68. Mandolfo, O., Parker, H., and Bigger, B. (2022). Innate Immunity in Mucopolysaccharide Diseases. Int. J. Mol. Sci. *23*, 1999.

69. Hampe, C.S., Eisengart, J.B., Lund, T.C., Orchard, P.J., Swietlicka, M., Wesley, J., and McIvor, R.S. (2020). Mucopolysaccharidosis Type I: A Review of the Natural History and Molecular Pathology. Cells *9*, 1838.

70. He, X., Zhang, Z., Xue, J., Wang, Y., Zhang, S., Wei, J., Zhang, C., Wang, J., Urip, B.A., Ngan, C.C., et al. (2022). Low-dose AAV-CRISPR-mediated liver-specific knock-in restored hemostasis in neonatal hemophilia B mice with subtle antibody response. Nat. Commun. *13*, 7275.

71. Xu, L., Lau, Y.S., Gao, Y., Li, H., and Han, R. (2019). Life-Long AAV-Mediated CRISPR Genome Editing in Dystrophic Heart Improves Cardiomyopathy without Causing Serious Lesions in mdx Mice. Mol. Ther. *27*, 1407–1414.

72. Peracha, H., Sawamoto, K., Averill, L., Kecskemethy, H., Theroux, M., Thacker, M., Nagao, K., Pizarro, C., Mackenzie, W., Kobayashi, H., et al. (2018). Molecular genetics and metabolism, special edition: Diagnosis, diagnosis and prognosis of Mucopolysaccharidosis IVA. Mol. Genet. Metabol. *125*, 18–37.

73. Brinkman, E.K., Chen, T., Amendola, M., and van Steensel, B. (2014). Easy quantitative assessment of genome editing by sequence trace decomposition. Nucleic Acids Res. *42*, e168.

74. van Diggelen, O.P., Zhao, H., Kleijer, W.J., Janse, H.C., Poorthuis, B.J., van Pelt, J., Kamerling, J.P., and Galjaard, H. (1990). A fluorimetric enzyme assay for the diagnosis of Morquio disease type A (MPS IV A). Clin. Chim. Acta *187*, 131–139.

75. Leal, A.F., Cifuentes, J., Torres, C.E., Suárez, D., Quezada, V., Gómez, S.C., Cruz, J.C., Reyes, L.H., Espejo-Mojica, A.J., and Alméciga-Díaz, C.J. (2022). Delivery and assessment of a CRISPR/nCas9-based genome editing system on in vitro models of mucopolysaccharidoses IVA assisted by magnetite-based nanoparticles. Sci. Rep. *12*, 15045.

76. Schneider, C.A., Rasband, W.S., and Eliceiri, K.W. (2012). NIH Image to ImageJ: 25 years of image analysis. Nat. Methods *9*, 671–675.

77. Chew, W.L., Tabebordbar, M., Cheng, J.K.W., Mali, P., Wu, E.Y., Ng, A.H.M., Zhu, K., Wagers, A.J., and Church, G.M. (2016). A multifunctional AAV-CRISPR-Cas9 and its host response. Nat. Methods *13*, 868–874.

78. Charlesworth, C.T., Deshpande, P.S., Dever, D.P., Camarena, J., Lemgart, V.T., Cromer, M.K., Vakulskas, C.A., Collingwood, M.A., Zhang, L., Bode, N.M., et al. (2019). Identification of preexisting adaptive immunity to Cas9 proteins in humans. Nat. Med. *25*, 249–254.